Anomalies in high-order harmonic generation at relativistic intensities

U. Teubner,[1,*] G. Pretzler,[2] Th. Schlegel,[3] K. Eidmann,[2] E. Förster,[1] and K. Witte[2]
[1]*Abteilung Röntgenoptik, Institut für Optik und Quantenelektronik, Friedrich-Schiller-Universität Jena, Max-Wien-Platz 1, 07743 Jena, Germany*
[2]*Max-Planck-Institut für Quantenoptik, Hans-Kopfermann-Strasse 1, 85748 Garching, Germany*
[3]*Institut für Kernphysik, Technische Universität Darmstadt, Schlossgartenstrasse 9, 64289 Darmstadt, Germany*
(Received 28 August 2002; published 30 January 2003)

High-order harmonic generation from a solid target surface has been investigated using femtosecond laser pulses focused to intensities greater than 10^{18} W/cm^2. The experiments show that the harmonics are very intense, with a conversion efficiency that is one or two orders of magnitude larger than that of harmonics generated in gases. Beside the observation of presently the shortest wavelength harmonics from femtosecond-laser solid target interaction, i.e., down to 22 nm, an anomaly has been observed in the harmonic spectrum. In contrast to the expected well-known continuous ''roll off'' of the high-harmonic orders, the harmonic intensity decreases with the increase of harmonic order, but in between shows minima which are significantly less intense than the neighboring harmonics. Furthermore, the order of the harmonic minima depend on target material. Additional calculations using numerical kinetic particle simulations and a simpler oscillating mirror model show that the physical origin of these modulations is an intricate interplay of resonance absorption and ponderomotive force which leads to a complex electron density profile evolution. Furthermore, this is emphasized by a spectral line analysis of the harmonics. In agreement with the theory, broad lines have been observed and, in particular for the harmonics in the minima, a complex interference structure is present.

DOI: 10.1103/PhysRevA.67.013816 PACS number(s): 42.65.Ky, 32.30.Jc, 52.70.Kz, 52.38.−r

I. INTRODUCTION

High-order harmonic generation is a method to accomplish intensive and coherent pulses at short wavelengths. This subject has been studied for more than a decade, mainly using gas jets for frequency conversion (see, e.g., [1–3]). However, there are several problems with those ''gas-harmonics.'' First, the maximum intensity of the harmonic emission is limited by the maximum laser intensity that could be applied because gas ionization has to be avoided. Second, high-order harmonic generation (HOHG) requires proper phase matching between the fundamental and the harmonics, so that recently gas-filled capillaries are used instead of gas jets [4].

An alternative method, which does not suffer from such problems, is to focus a laser pulse to high intensity on the surface of a solid target. At suitable conditions, a spectrum of harmonics is observed in the direction of the reflected laser pulse. This type of HOHG offers two advantages: First, in contrast to the gas jet experiments which allow for odd-order harmonics only, even and odd harmonics are emitted and second, no limitation of laser energy is known so far which promises scaling up to very high fluxes of the harmonics.

Originally such experiments were done using nanosecond laser pulses [5], but with the advent of the chirped pulse amplification (CPA) technique [6] and the availability of intense enough picosecond and femtosecond pulses, mostly ultrashort pulses have been applied for HOHG. In the following, we will restrict to these harmonics from solid surfaces and, in particular, we will concentrate on HOHG by means of femtosecond laser pulses which were observed for the first time in experiments by Kohlweyer *et al.* [7] and von der Linde *et al.* [8].

In a simplified model, the physical principle of such HOHG is the oscillation of the mirrorlike target surface which is caused by the large ponderomotive pressure of the light pulse or driven additionally by the resonant plasma wave in the case of *p*-polarized laser light (the ''moving mirror model'' [9,10]). Later on, further detailed simulations by the same authors and by Gibbon [11] have shown a substantial increase of the harmonic order and harmonic intensity at relativistic intensities ($>10^{18}$ W/cm^2) and an inherent coupling of the phases of the harmonics. In experiments by Norreys *et al.* and Chang *et al.* with 2.5 ps laser pulses, harmonics up to 75th order of the 1053-nm fundamental were measured [12,13]. However, in significant contrast to the theoretical predictions [9–11] the observed source parameters showed that the moving mirror model could not be simply applied at their conditions (e.g., the harmonic emission was nearly isotropic instead of being in specular direction of the fundamental laser light and spectrally broader than expected). In this work and the more recent experiment of Watts *et al.* [14] the situation for this interaction with high-intensity *picosecond* laser pulses was characterized by large preplasma, modified and steepened by the the light pressure [15].

There is a large potential for applications for which it may be interesting to confine the harmonics emission to a small solid angle and thus to increase efficiency and spatial coherence of HOHG. These goals and, of course, clean and nonambiguous experimental conditions, can be achieved by using even shorter pulses (pulses of the order of a hundred *femtoseconds* or less [16]). In this case, the femtosecond-laser solid target interaction (FSI) occurs directly with the critical surface which has a very steep density gradient. Zepf

*Corresponding author. Email address: teubner@ioq.uni-jena.de

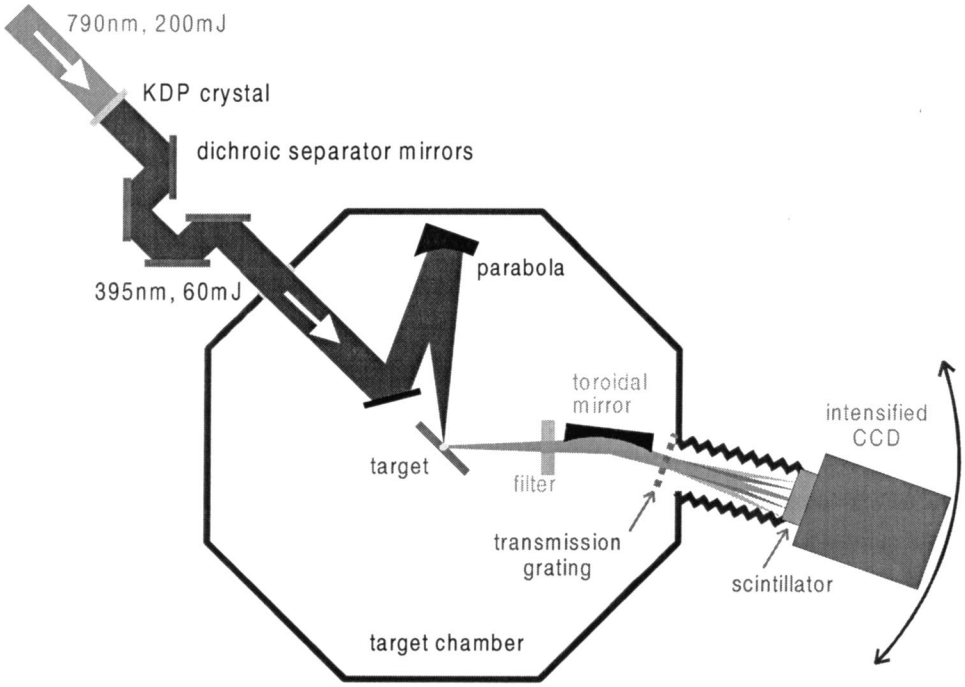

FIG. 1. Experimental setup.

et al. [17] have shown that depending on the prepulse level and the contrast ratio (pulse-peak intensity to that of the background or prepulse, respectively) FSI harmonic emission becomes more efficient if the laser pulse interacts with a very steep density gradient at the critical surface.

II. EXPERIMENTAL SETUP

In this work we have extended those previous experiments by performing measurements on HOHG using very clean laser pulses. To achieve this, we have used frequency-doubled pulses from the ATLAS-2 laser system at the Max-Planck-Institut für Quantenoptik which is a 10-Hz Ti:sapphire laser emitting laser pulses of 230-mJ energy and 130-fs duration. These laser pulses at $\lambda = 790$ nm wavelength have an intrinsic prepulse of $\sim 10^{-4}$ (~ 1 ps ahead of the peak) and an amplified spontaneous emission (ASE) pedestal of less than 10^{-8} compared to the main pulse intensity [18]. Both effects are strong enough to create a plasma at the target surface. In such a case, the main pulse would interact with a preplasma extended to several microns. To avoid this situation, the laser light was frequency doubled to $\lambda_0 = 395$ nm and thus the prepulse level decreased to less than 10^{-7} so that preplasma formation was avoided (with the expense of a reduced pulse energy of ~ 60 mJ). The remaining unconverted fundamental light was reduced by a factor of greater than 10^7 by a set of four multilayer mirrors. Therefore on the target, plasma creation was only possible by the main pulse itself which leads to the interaction of the laser pulse peak with a very dense plasma (solid state density) with an extremely steep density gradient of the order less than 1 μm [17,19,20].

An $f/2.5$ off-axis multilayer-coated parabolic mirror was used for focusing. The focal spot was carefully characterized by a direct 50:1-magnification setup. The focus consisted (a) of a central near-diffraction-limited spot (~ 3.6 μm diameter) containing more than half of the pulse energy and peak intensities up to many times 10^{18} W/cm^2 and (b) of a broader structure farther around, such that the usual value of 86% of the energy was found within a diameter of 12.8 μm. The values, I_L, given for intensity throughout this paper, mean the average intensity within the full central spot (diameter ~ 5 μm) yields a maximum intensity of 1.5×10^{18} W/cm^2, which is almost a factor of 10 higher than that achieved before [17]. By changing the timing of the pump pulse in the amplifier chain, I_L could be varied between 10^{17} and 1.5×10^{18} W/cm^2 so that, for comparison, additional measurements could be made at lower intensities.

The laser pulses were incident p polarized under an angle $\alpha = 45°$ on solid slab targets of various materials (solid aluminum, copper, fused silicon, and Sigradur, a glasslike carbon modification of density $\rho = 1.4$ g/cm^3). The target was mounted on an *xyz* translation unit and was moved between consecutive shots to always present a fresh surface.

Single and multishot spectra in the wavelength region from 10 to 80 nm were recorded by a single-shot transmission grating spectrograph [(TGS); see Fig. 1]. The TGS which consists of a toroidal mirror at gracing incidence, a free-standing gold grating, and a two-dimensional detector (Proscan GmbH, Germany) was mounted in specular direction of the fundamental, i.e., at 45° with respect to the target normal (details of the TGS are described in Refs. [21] and [22], respectively). A 100-nm-thick aluminum filter was mounted in front of the TGS to discriminate against the laser fundamental. Two different gratings have been used: first, for the observation of an extended wavelength range a grating with 1000 lines per mm [Dr. Johannes Heidenhain GmbH, Germany (TG1)] and second, a 5000 lines per mm grating [X-Opt Inc., Florida (TG5)] for a detailed measurement of the high harmonics with a five times better spectral resolution. These large aperture gratings (10 mm$\times$4 mm) are

mounted on a support grid of a 33-μm and 4-μm period, respectively. The contribution of higher diffraction orders in the spectrum has been found to be less than a few percent for TG1 and less than 17% for TG5.

The detector consists of a Gd_2O_2S:Tb scintillator [23] that converts the extreme ultraviolet (XUV) photons to visible light, a 25-mm-diam microchannel plate which is fiber-coupled optically to the scintillator and a charge-coupled device (CCD) for the readout. Although due to its high efficiency the TGS is able to measure a single-shot spectrum, five to ten spectra were averaged for each individual measurement to achieve better reproducibility.

The observed spectral range could be easily changed by moving the detector position (Fig. 1). Wavelength calibration is easily done using the well known Lyman-α (at 3.4 nm) and helium-α (at 4 nm) lines of a carbon target and the K edge of the aluminum filter at 17 nm. In addition, the wavelength of each harmonic line could be checked from the higher orders of the line diffracted by the support grid in the y direction [Fig. 2(a)]. Altogether, this gives an absolute accuracy of the wavelength of $\delta\lambda/\lambda = 0.4\%$. The total accessible spectral window for the harmonics ranges from 16 to 82 nm. For lower wavelengths the reflectivity of the gracing incidence mirror R_m is strongly reduced. Between 7 and 17 nm and for wavelengths greater than 82 nm the radiation is blocked by the 100-nm-thick aluminum filter.

III. EXPERIMENTAL RESULTS

A. Harmonic spectra

Figure 2(b) shows a typical spectrum from a from a glass target, measured with TG1 at a laser intensity of $I_L = 1.2 \times 10^{18}$ W/cm^2 (solid line). This spectrum shows no significant second-order diffraction and is corrected for the transmission of the aluminum filter T_{Al} (dashed line; the K edge of the filter at 17 nm in first diffraction order is indicated by "K1") [24] and the scintillator efficiency η_{scint} (dotted line, in arbitrary units) [23,25]. Here, high-order harmonics are clearly visible up to 13th order of the $\lambda_0 = 395$ nm fundamental. At even shorter wavelengths further harmonics are sitting on a background emission originating from the hot plasma (ionic spectrum and continuum radiation, in the following brief "plasma emission"; this is indicated by "P1") [26]. To show this more clearly Fig. 2(c) displays a spectrum measured with TG5 at slightly higher laser intensity. After correction for filter transmission, scintillator efficiency, and background subtraction, one nonambiguously can recognize harmonics up to the 18th or 19th order. Presently this is the shortest wavelength harmonic obtained from the interaction of *femtosecond* laser pulses with solid targets.

From Fig. 2 one can see that the intensity of the harmonics is strongest for the lowest order and decreases to shorter wavelengths (6th to 10th order). This corresponds to the well-known continuous "roll-off" as expected [9]. However, after reaching a minimum (11th order), the harmonic emission becomes stronger again. The minimum at the 11th harmonic is well reproducible [27]. It does not depend on the grating or any other part of the diagnostics, such as T_{Al}, R_m, or η_{scint}, because between 25 and 60 nm the spectral response of these components is steady and flat [23–25] [Fig. 2(b)]; for larger wavelengths a correction for filter transmission is important; see e.g., Fig. 3: the fifth harmonic seems to be much too weak since there no correction was applied). Moreover, the real nature of this anomaly can be seen from Fig. 3, which shows spectra not effected by any correction: repeated measurements with the same diagnostics but different target materials, but otherwise the same experimental conditions, also showed variations of the position of the harmonic minimum. In particular, in contrast to glass [Figs. 2 and 3(c)], the minimum for carbon [Fig. 3(a)] occurs at the 9th harmonic and in the spectra of the two metals aluminum and copper, no minimum could be observed.

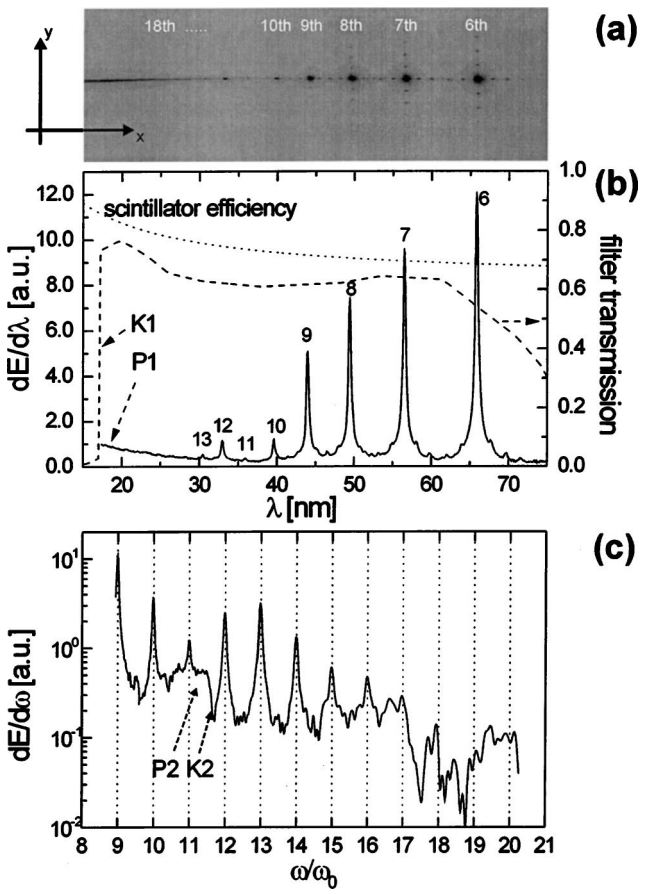

FIG. 2. High-order harmonic spectrum of a glass target measured at $I_L = 1.2 \times 10^{18}$ W/cm^2. (a) Raw data as seen on the CCD chip. Horizontal: harmonic spectrum; vertical: higher orders from diffraction at the support grid of TG1 (in arbitrary units). (b) Harmonic spectrum (energy per wavelength interval) measured with TG1. (c) Extended region of the highest harmonics (energy per frequency interval), measured with TG5 at $I_L = 1.5 \times 10^{18}$ W/cm^2 [27]. In (a) to (c) ten shots were accumulated. "$P1$" indicates the plasma emission in first diffraction order and "$K1$" the K edge of the Al filter at 17 nm in first diffraction order. $P2$ and $K2$ are the corresponding second orders.

To get rid of any background from both plasma emission and higher diffraction orders of TG1 and TG5 we have corrected the spectra for T_{Al} and η_{scint} and integrated all harmonic lines separately. Plotting these integrals as a function of harmonic order, Fig. 4 shows even more clearly that for

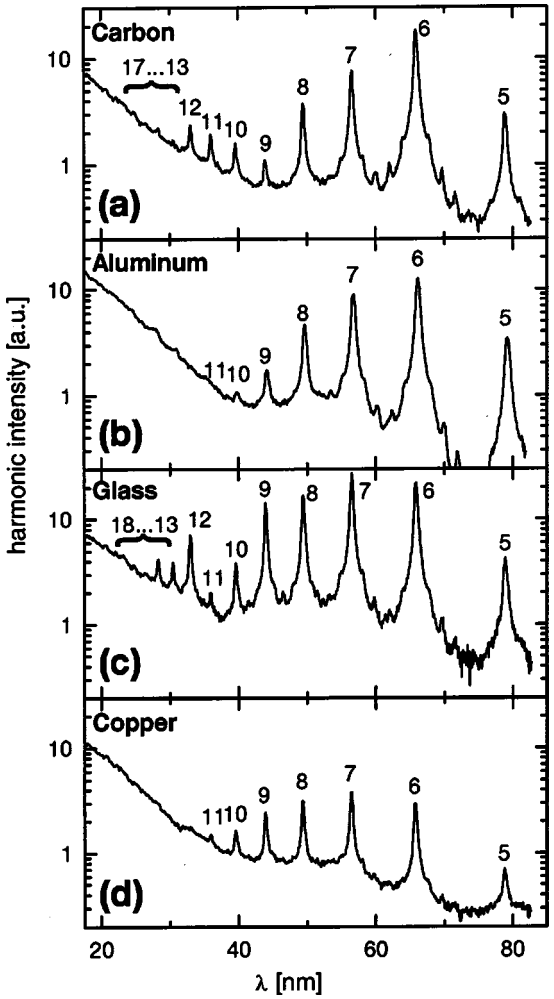

FIG. 3. High-order harmonic spectra for different target materials irradiated with $I_L = 1.5 \times 10^{18}$ W/cm^2 laser pulses (all measured with TG1; here no correction was applied for T_{Al} and η_{scint}). Ten shots were accumulated: (a) highly polished glassy carbon (SIGRADUR), (b) unpolished aluminum, (c) glass, and (d) polished copper.

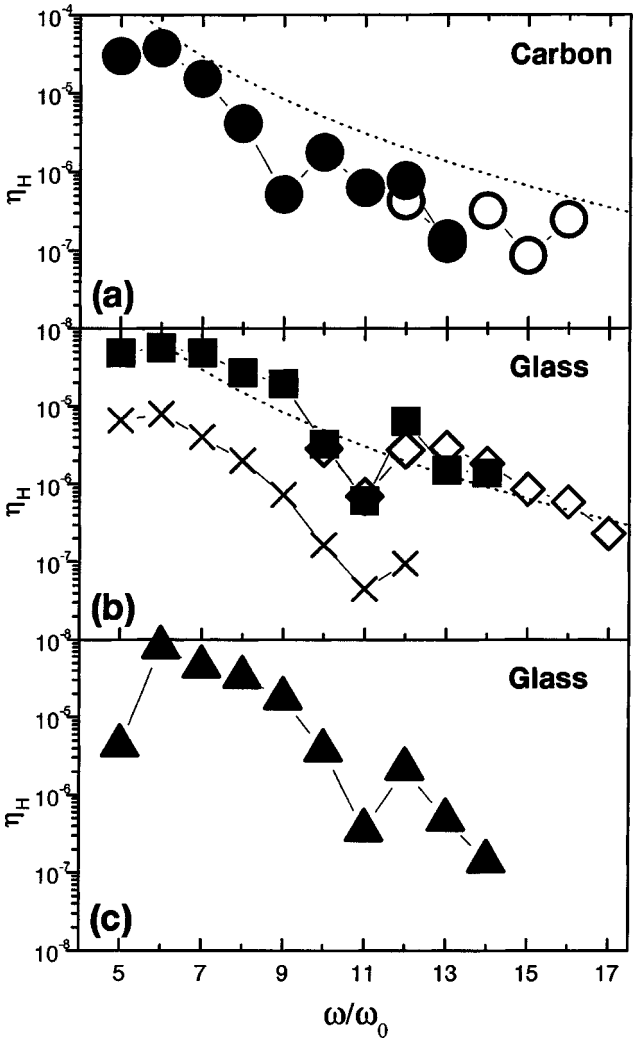

FIG. 4. Harmonic efficiency η_H as a function of harmonic order. (a) Carbon and (b) and (c) glass. Solid (open) symbols: measurement with TG1 (TG5). Circles and squares: measurement without prepulse; crosses: measurement with prepulse (see text) ($I_L = 1.5 \times 10^{18}$ W/cm^2). For comparison (c) shows a measurement at 36% reduced intensity (no prepulse). The dashed line in (a) and (b) corresponds to the harmonic efficiency from Eq. (1). The symbol size in the direction of the ordinate corresponds to the shot-to-shot fluctuations. All data are corrected for T_{Al} and η_{scint}. The accuracy of the absolute values of η_H is within one order of magnitude.

carbon there is even a real modulation with several minima apparent, namely at the 5th, 9th, 11th, 13th, and 15th harmonic instead of only one at the 11th (and maybe the 5th) in the case of glass.

Here we would like to emphasize the importance of clean experimental conditions if this modulation should be clearly present. This is illustrated by a supplementary measurement where an additional well controlled small prepulse (395-nm wavelength, 130-fs pulse duration, intensity 3×10^{14} W/cm^2) was applied 200 ps before the main pulse. In this case a preplasma is generated, which in this case has a scale length of approximately 3 μm (estimated by calculations with the hydro code MULTIFS [28]).

Similar to the detailed investigations of Zepf *et al.* [17] and Tarasevitch *et al.* [16], we have observed that the prepulse strongly reduces the overall harmonic emission [this is even more pronounced than the effect from reducing I_L, Fig. 4(c)]. Moreover, Fig. 4(b) shows that the negative effect of the prepulse increases with harmonic order: the 5th to 7th harmonic are reduced by a factor of 7 to 12, whereas the 9th harmonic is reduced by a factor of 27 and the 12th by a factor of 30 to 70. At the same time, the background below 40 nm (i.e., the plasma emission) strongly increases, too (compare [29]), and it is difficult to discriminate harmonics above the 11th order from it.

B. Efficiency

Figure 3 also shows that the harmonics are very intense. In particular for the dielectric target materials [Figs. 3(a) and 3(c)], the harmonic emission significantly exceeds the plasma emission (marked as "*P*1" in Fig. 2). A rough estimate of the conversion efficiency η_H into harmonic emission was made by comparison of the relative signals of the har-

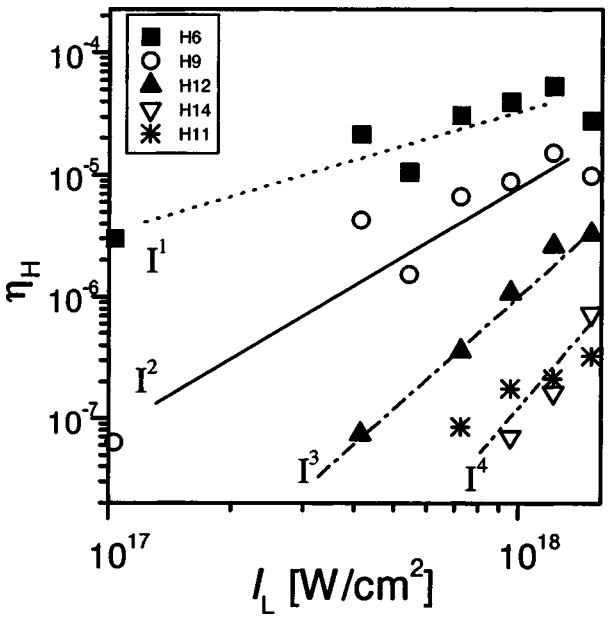

FIG. 5. Harmonic efficiency η_H as a function of laser intensity for a glass target for selected harmonics (squares 6th, circles 9th, up triangles 12th, down triangles 14th, and stars 11th harmonic, which is the minimum). The lines indicate a scaling with I^1 to I^4. The data are corrected for T_{Al} and η_{scint}. The accuracy of η_H is within one order of magnitude.

monics to that of the carbon Lyman-α line emission measured with the same setup during the same experiment. In addition, we would like to mention that the duration of the harmonics is expected to correspond to the laser pulse duration of 130 fs while the plasma emission has a duration of several picoseconds [19].

Taking into account the known conversion efficiency $\eta_{\text{Ly-}\alpha}$ for this carbon line (a conservative estimate is $\eta_{\text{Ly-}\alpha} \approx 10^{-4}$ to 10^{-3} [22,30]), the integral over the carbon Lyman-α line and the individual harmonic lines, respectively (all in the *same arbitrary units*), the solid angle of emission (2π sr for the carbon line; the same solid angle for reflected laser light and harmonics, i.e., given by the $f/2.5$ optics) and the wavelength dependence of the TGS throughput (filter transmission, mirror reflectivity, grating efficiency, scintillator efficiency, etc.) we obtain $\eta_H > 10^{-5--4}$ for the for the 6th harmonic (see Fig. 4). For comparison, the dashed line shows the scaling of the efficiency

$$\eta_H \approx 9\times 10^{-5}\left(\frac{I_L\lambda^2}{10^{18}\ \mathrm{W\,cm^{-2}}\ \mu\mathrm{m}^2}\right)^2\left(\frac{N}{10}\right)^{-5} \qquad (1)$$

which corresponds to the empirical relation given by Gibbon [31], Eq. (37). If one neglects the modulations which are not included in this relation, approximate agreement can be seen. This shows that HOHG on solid targets may be much stronger than that from gases, where a typical value for harmonics in the same wavelength range is $\eta_H \approx 10^{-6}$. This is also an upper limit because higher laser intensities would cause strong ionization of the gaseous medium and thus suppress HOHG [2,32] and therefore have to be avoided.

Figure 5 shows the harmonic intensity as a function of laser intensity for a glass target. One can easily see a strong increase of η_H with I_L. At relativistic intensities (approximately $I_L > 10^{18}$ W/cm^2) the short wavelength harmonics do scale with I_L^4 or more. This is very promising with respect to achieve intensive short wavelength harmonics as mentioned before. Furthermore, Fig. 5 shows that the harmonic of the minimum (H11) scales much weaker with I_L in contrast to the other harmonics.

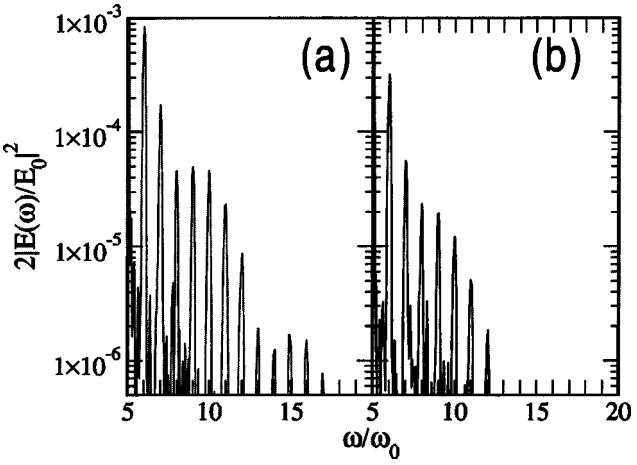

FIG. 6. PIC simulations of high harmonic spectra from a carbon target at $a_0=2$ (a) and $a_0=1.8$ (b), respectively.

We also would like to mention that the previously measured efficiency of the 10th harmonic of 800 nm obtained at a laser intensity which is one order of magnitude lower than that of the present work is approximately 10^{-6} [16]. If one compares harmonics at the same wavelength, e.g., the 10th and 5th harmonic, respectively, measured at the different intensities and wavelengths of both experiments, relation (1) yields a slightly larger efficiency for the present work as observed in our experiment.

IV. SIMULATIONS

A. Kinetic particle simulations

The experimental situation was modeled by means of the one-dimensional 1D particle-in-cell code LPIC [9]. Oblique incidence of the laser radiation on the target is treated by applying the relativistic ''boost frame'' transformation [33]. In all simulations, initial electron temperatures T_e between 300 and 600 eV and cold ions were assumed. The target was approximated as a thin layer of laser wavelength thickness λ_0 with vacuum layers $3\lambda_0$ in front and behind it. This geometry of the simulation box provides particle kinematics with only few reflections on the box boundaries. We used *p*-polarized $\sin^2$-shaped laser pulses with 100 fs duration and an angle of incidence $\alpha=45°$ on the target. Fourier-transformed fields were looked at different positions along the laser propagation path. To compare with experimentally obtained spectra, we show Fourier transforms of the reflected light calculated at the box entrance (laser side).

Figure 6 demonstrates the influence of the incident laser intensity in units $a_0 = eE_0/m_e\omega_0 c$ for a carbon target with an initially steplike density profile. E_0 is the electric field of the

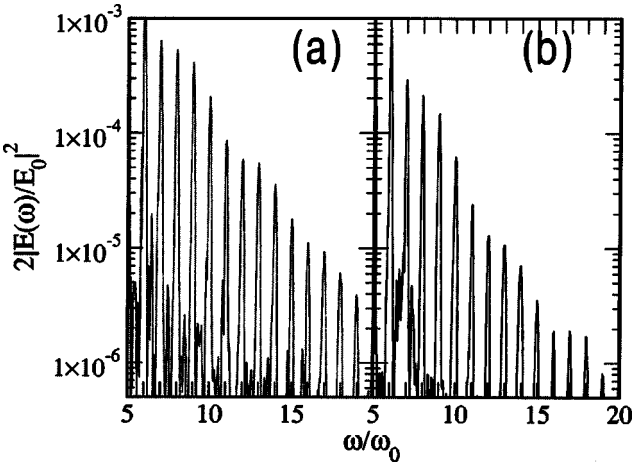

FIG. 7. PIC simulations of high harmonic spectra from a glass target at $a_0=2$ (a) and $a_0=1.8$ (b), respectively.

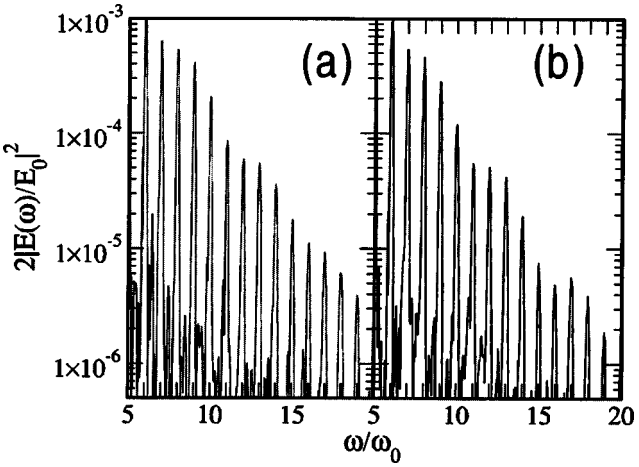

FIG. 8. PIC simulations of high harmonic spectra from a glass target for low and high ionization degree: $M_i/M_e=37000$ (a) and $M_i/M_e=7000$ (b), respectively.

laser pulse, m_e the electron mass, ω_0 the angular frequency of the 395-nm laser pulse, and c the velocity of light. Above some value $a_0\sim 2$ [Fig. 6(a)], which corresponds to a mean focal intensity $I_L\approx 2.5\times 10^{19}$ W/cm^2 for $\lambda_0=395$ nm, the peak intensities of the high harmonics become modulated. Already a small decrease in laser intensity [Fig. 6(b)] removes the modulations. A similar effect on harmonic intensities is obtained when the initial target density profile is varied. In the case of an initial plasma scale length $L/\lambda_0 \geqslant 0.1$, intensity modulations in the calculated spectra were reduced or disappeared. This result suggests that the high-contrast ratio in our laser pulse indeed was a decisive prerequisite for the observation of the anomalies in the detected harmonic spectra.

The modeling also clearly shows the role of the initial target density. At the surface of materials with large n_i/n_c (n_i is the ion density and n_c is the critical electron density; for carbon this ratio is about 16), weaker high harmonics will be generated than in the case of targets with smaller density, e.g., glass (see Fig. 7). This fact is in plausible agreement with the oscillating mirror model (see [9]). A lower density implies a smaller restoring force; therefore, larger amplitudes of the electron surface oscillations are responsible for harmonic generation.

In addition, we analyzed the influence of target ionization on harmonic spectra. Because the used PIC scheme does not treat ionization processes explicitly, we use an indirect form of description through ion mobility. A higher ionization degree in the quasineutral ensemble of electrons and ions is equivalent to higher ion mobility, or smaller ratio M_i/M_e of macroparticle masses. We observe an enhancement of the modulations in harmonic peak intensities with growing ion mobility as shown in Fig. 8. Qualitatively, the result depicted in this figure is close to our experimental observation, although the local intensity minimum (at the 11th harmonic) is less pronounced.

An examination of the density profile oscillation driven by the electric field and the ponderomotive force, respectively, showed that the movement of the critical surface shows a deviance from a pure harmonic oscillation. However, the PIC simulations showed a general discrepancy to the experimental spectra: To observe high-harmonic orders, e.g. $\geqslant 10$ in glass, higher laser intensities are more necessary than available in the experiment. Also the difference of the orders where the harmonic signal reaches its relative minimum is different from what is observed in the experiment. We note that these discrepancies are also present in the work of Watts *et al.* [14] and the reason is not understood yet.

B. Oscillating mirror model

Thus to get more insight in the harmonic generation process at the critical surface of the electron density, we tried to get much simpler access to the relevant physics and came back to the oscillating mirror model [9,10,34]. Then the complex relativistic motion of the electrons on a classically behaving ion background can be described in the framework of a cold relativistic plasma fluid model developed by Lichters [9] for the general case of oblique laser incidence. The equation for the longitudinal electron movement (along with laser propagation) in the moving frame [33] reads

$$\frac{d}{dt}\beta_x=\frac{c}{\gamma}(1-\beta_x^2)\frac{\partial\varphi}{\partial x}-\frac{1}{\gamma^2}\left(c\frac{\partial}{\partial x}+\beta_x\frac{\partial}{\partial t}\right)\left(\frac{\mathbf{a}^2}{2}-a_y\tan\alpha\right) \tag{2}$$

with the notations $\beta_x=v_x/c$ as the longitudinal fluid velocity, $\gamma=\sqrt{1+(p/mc)^2}$, $\mathbf{a}=e\mathbf{A}/mc$ the dimensionless vector potential ($\mathbf{A}$ is the vector potential), and $\varphi=e\Phi/mc^2$ the scaled dimensionless scalar potential.

We distinguish three force terms on the right-hand side. The first term describes the longitudinal charge separation, which can be caused by the corresponding electric field component of a *p*-polarized laser wave at oblique incidence. The second term contains the ponderomotive force

$$F_p=-\frac{mc^2}{\gamma}\frac{\partial}{\partial x}\frac{\mathbf{a}^2}{2}. \tag{3}$$

It causes a surface motion with twice the laser frequency. A third term, arising again at obliquely incident laser illumination only, is a Lorentz force. It follows from the action of the magnetic field $B_z \propto \partial A_y/\partial x$ on a transverse surface current driven by the corresponding electric field component E_y. It will excite plasma surface oscillations with laser frequency similar to the longitudinal charge separation term. Therefore, we describe the oscillation coordinate $X(t)$ in a simplified form as

$$X(t) = X_\omega \sin(\omega t - \varphi_\omega) - X_{2\omega} \cos(2\omega t - \varphi_{2\omega}) \tag{4}$$

(note: at oblique incidence in the boosted frame the frequency ω is lower than in the laboratory frame, $\omega = \omega_0 \cos\alpha$). If the frequency of the light pressure is close to the plasma frequency, $2\omega \approx \omega_p$, we set approximately $\varphi_\omega \approx 0$ and $\varphi_{2\omega} \approx \pi/2$. In a next step, we analyze the influence of the oscillating surface, where the incoming light will be reflected, on the reemission process. Here one has to account for time retardation. An observer (spectrograph) will detect the reflected light at a shifted time

$$t_{\mathrm{ret}} = t - \frac{X(t)}{c} \tag{5}$$

with

$$X(t) = \frac{2}{\cos\alpha}(X_\omega \sin\omega t + X_{2\omega} \sin 2\omega t). \tag{6}$$

The observer position is neglected here because it contributes only a constant shift in time. The amplitudes X_ω and $X_{2\omega}$ could be directly estimated from the resonantly enhanced electric field at n_c and the ponderomotive force, respectively. But we have to note that there is an upper limit for the amplitudes because the maximum speed of the ''oscillating mirror'' has to be lower than c which limits X_ω and $X_{2\omega}$ to a fraction of λ_0.

We also would like to mention that at relativistic intensities due to the relativistic kinematic motion, even further components $X_{3\omega}\sin(3\omega t)$, etc., appear, which will even enhance the harmonic emission, in particular the higher orders. However, this is not the dominant part in Eq. (6) and does not change the basic nature of our discussion.

Thus we have restricted the first two amplitudes and estimated X_ω and $X_{2\omega}$ for the parameters of the experiment ($I_L = 2\times10^{18}$ W/cm^2, $\lambda_0 = 395$ nm, 100 fs pulse with a Gaussian envelope, approximately bandwidth limited, i.e., spectral bandwidth $\Delta\lambda_0 = 2.8$ nm [35]) and calculated the optical path as a function of time and the corresponding spectrum [$kx_{\mathrm{ret}} = (t - t_{\mathrm{ret}})c/\lambda_0$; Figs. 9(b) and 10(b)].

As an example, Fig. 9(b) indicates a complex motion of the critical surface in the vicinity of the pulse maximum, whereas much before or later in time, the motion is much weaker and sinusoidal (in principle, our PIC simulations also have shown a deviance from a pure harmonic oscillation). But depending on the ratio $X_\omega/X_{2\omega}$ the motion may be even be more complicate: in Fig. 9(a) we have reduced this ratio and Fig. 9(c) shows the effect when $X_\omega/X_{2\omega}$ is increased.

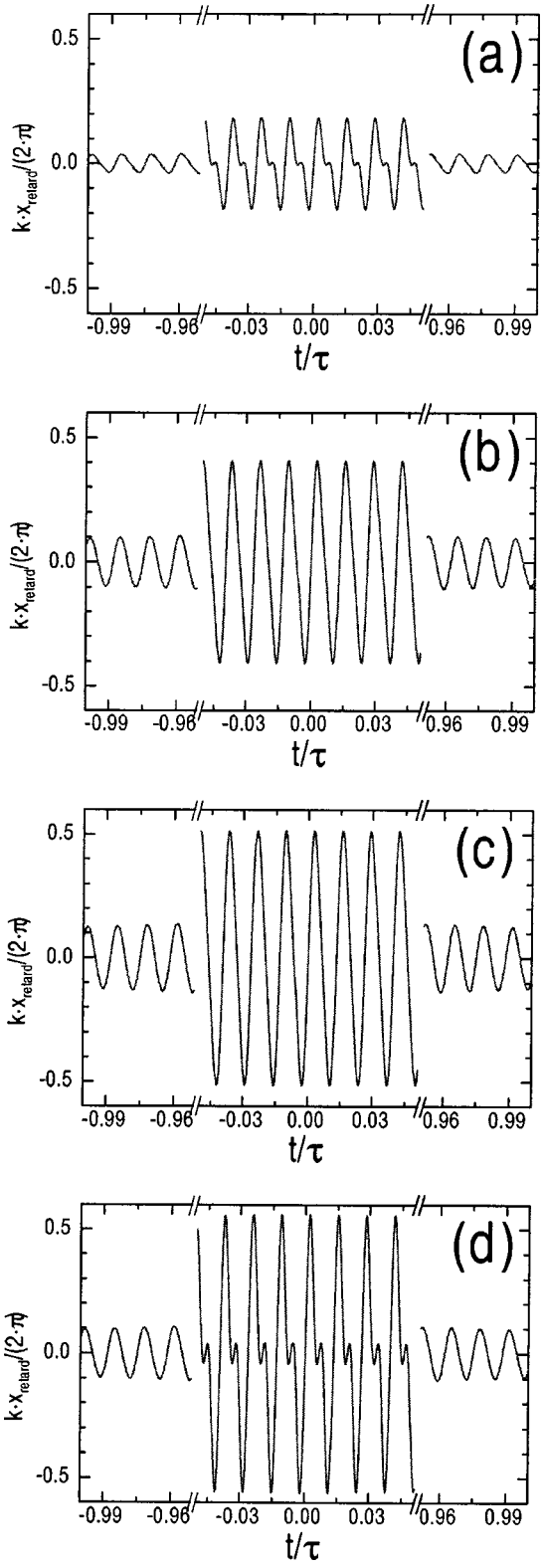

FIG. 9. Change of the optical path with time due to retardation, calculated with the oscillating mirror model. (a) $X_\omega/X_{2\omega} = 2$, (b) $X_\omega/X_{2\omega} = 5$, (c) $X_\omega/X_{2\omega} = 6$. In (a) to (c) we assumed an approximately constant scale length $L/\lambda_0 = 0.03$. In (d) $X_\omega/X_{2\omega} = 5$, but in addition it is assumed that due to the strong ponderomotive force, the original scale length is reduced during the interaction [see the inset in Fig. 10(d)]. The pulse maximum is at $t = 0$.

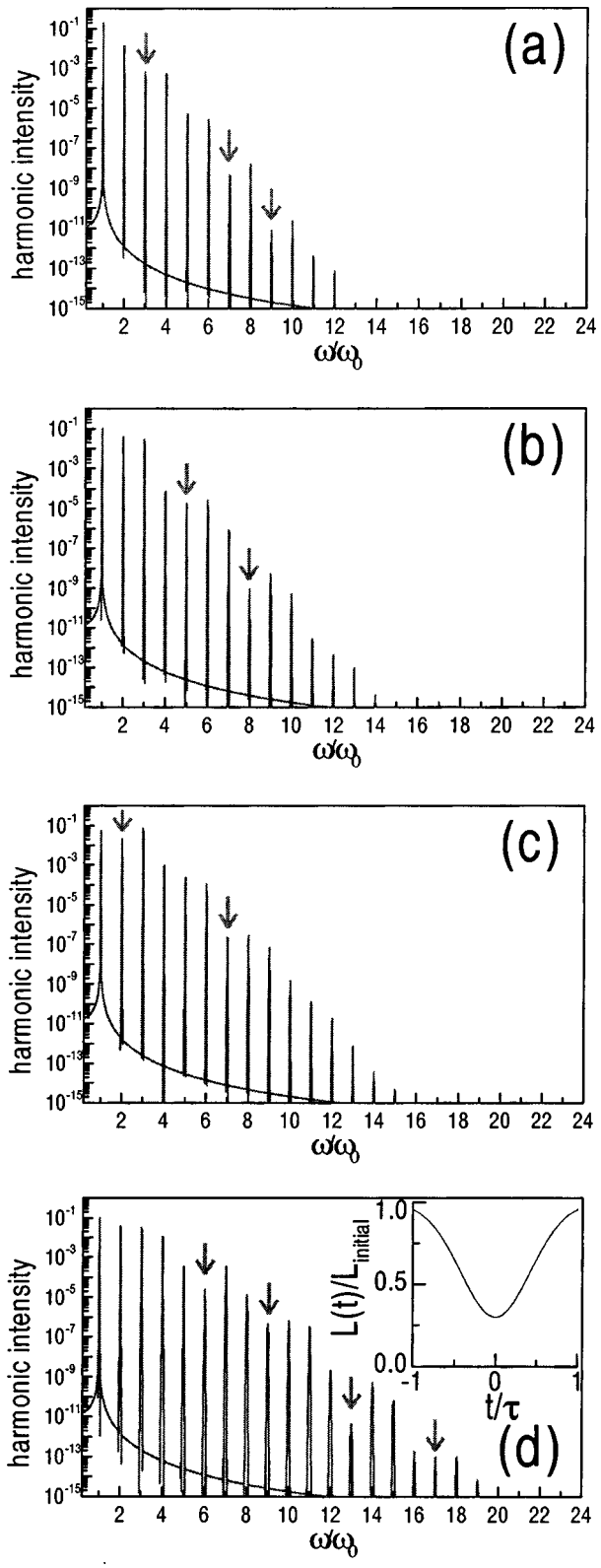

FIG. 10. Harmonic spectra calculated with the oscillating mirror model. The spectra in (a) to (d) correspond to the situations shown in Fig. 9. In (d) it is assumed that the change of scale length follows approximately the envelope of the laser pulse (see inset). The positions of the relative minima are indicated by arrows.

Another situation is shown in Fig. 9(d) where the effect of a transient change of the scale length is shown.

Fourier transformation leads to the spectra shown in Fig. 10 which, *in principle*, are not too different from what we observed in our experiment. One can clearly see the typical ''roll-off'' but with relative minima in between. The intensity of the harmonics and the positions of the minima depend on the actual experimental condition, which manifests in the amplitudes X_ω and $X_{2\omega}$ and their ratio which is of large importance. This may also explain the observed difference in the spectra obtained from different target materials (Fig. 3): in the case of lighter elements due to lower inertia, the scale length L will change much more during the interaction than for heavier elements. In this case a glass target would lead to a spectrum similar to Fig. 10(b) whereas a carbon spectrum would more correspond to Fig. 10(d) which shows more and also more pronounced minima (compare to Fig. 3 and Fig. 4).

The difference in the harmonic spectra of the dielectrics (glass and C) on one hand and the metals (Al and Cu) on the other hand is not well understood, in particular because the density of glass and Al is approximately the same but the differences in the spectra are significant [Figs. 3(b) and 3(c)]. A possible explanation may be the different enhancements of the electric field at n_c due to the different values of the dielectric function and the electron-ion-collision frequency. In this case X_ω will be different. Consequently, not only the total efficiency of harmonic generation and the number of harmonic orders will be altered, but also the interplay of resonance absorption and ponderomotive force which manifests in $X_\omega/X_{2\omega}$.

V. LINE ANALYSIS

The complex motion of the critical surface calculated in Sec. IV B is supported by the line-shape analysis of the harmonics. In particular, we have calculated the line profiles from the simulated spectra and compared to the experiment. As an example, Fig. 11 shows the shapes of the spectra from Fig. 10(b) and Fig. 10(d), respectively.

A typical line which is not a line in the minimum is shown in Figs. 11(a) and 11(c). It can be seen that the lines are relatively broad and slightly exceed the bandwidth expected from nonlinear optics $\Delta\lambda_N=\Delta\lambda_0 N^{-3/2}$, where $N\equiv\omega/\omega_0$ is the harmonic order and $\Delta\lambda_N$ the width of the Nth harmonic. As discussed by Lichters [9], the slightly larger linewidth in Fig. 11(c) when compared to Fig. 11(a) is due to a redshift of the harmonic emission during profile steepening (transient decrease of L) and the consecutive blueshift later on [see the inset of Fig. 10(d)]. Here we would also like to mention that due to plasma expansion (or compression), there might be an additional absolute shift of the harmonic wavelengths. However, from the absolute accuracy of the wavelength of the lines (i.e., $\delta\lambda/\lambda=0.4\%$, see the end of Sec. II) one can estimate an upper limit for the shift of the Nth harmonic of $|\Delta\omega|/\omega=0.4\%$ and for the corresponding velocity of $|v_p|<10^8$ cm/s.

In contrast to the normal lines, the lines in the minima

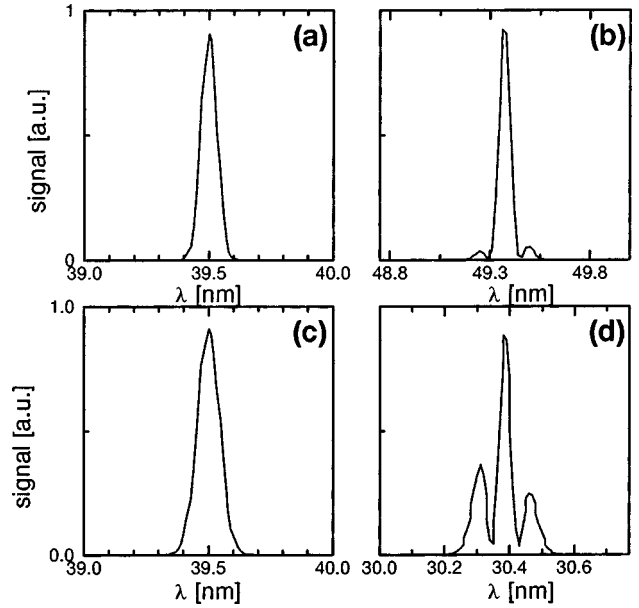

FIG. 11. Calculated line profiles from spectrum Fig. 9(b): (a) 10th harmonic (normal line), (b) 8th harmonic (minimum line). Calculated line profiles from spectrum Fig. 9(d): (c) 10th harmonic (normal line), (d) 13th harmonic (minimum line).

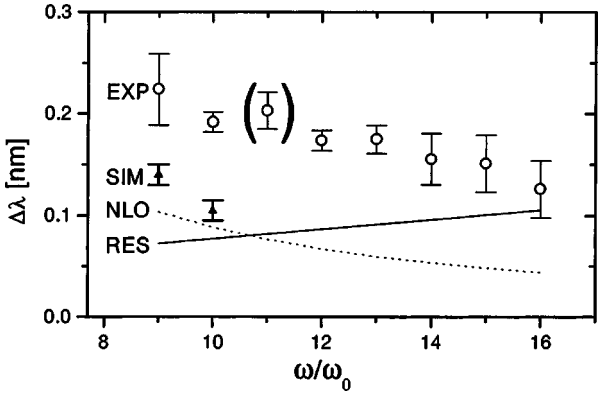

FIG. 12. Measured spectral linewidth [full width at half maximum (FWHM)] of the harmonics as a function of harmonic order for a glass target [from the spectrum in Fig. 2(c)]: ''EXP.'' The spectral resolution ''RES'' is shown as a solid line. For comparison the dotted line corresponds to a bandwidth as expected from nonlinear optics (''NLO''). As an example the triangles show what is expected from the oscillating mirror model (''SIM''). The brackets around the data experimental point of the 11th harmonic are because this is a ''minimum line'' where the designation of a FWHM is not sufficient.

have a more complicated structure and, in particular, wings are present beside the line center [Fig. 11(b), from the spectrum shown in Fig. 10(b)]. These wings indicate complex interference effects due to the complex motion of the critical surface. They are enlarged when the motion becomes more complicated [Fig. 11(d); they correspond to the more complicated situation shown in Figs. 9(d) and 10(d)].

Such shapes were also observed in the experiment. A more detailed line measurement was done using TG5. Although during this experiment the spectral resolution was limited to $\Delta\lambda_{res} \approx 0.1$ nm (due to the defocusing of TGS, $\Delta\lambda_{res}$ slightly depends on λ), it was found that the measured width of the harmonics significantly exceeds $\Delta\lambda_{res}$. As an example, Fig. 12 shows the relative width of the harmonics from a glass target as a function of N [from spectrum Fig. 2(c)]. One can recognize that if one takes into account $\Delta\lambda_{res}$, the linewidths calculated from the oscillating mirror model are in good agreement with the measured linewidths. We would like to note that within the experimental accuracy the linewidth is independent of target material and laser intensity [36].

The measured line profiles are displayed in Fig. 13. In Fig. 13(a) the 10th harmonic is plotted as an example for a typical normal line. One can see that the spectral width is significantly larger than the spectral resolution indicated by the arrows. The spectral shape agrees well with the shape of the simulated line from the oscillating mirror model when folded with a Lorentzian spectrometer function.

The measured ''minimum lines'' are very weak and, of course, strongly affected by noise. However, Fig. 13(b) shows that also these lines may show wings, which are separated by more than $\Delta\lambda_{res}$ from the central part of the line.

Finally we would like to mention that the large width of the ''normal'' harmonic lines in the frequency domain corresponds to ultrashort pulses in the time domain. In particular, the simulation with the oscillating mirror model shows that the typical temporal width of ''normal lines'' is approximately 30% of the laser duration. For the ''minimum lines'' the situation is different. Depending on the actual parameters, the temporal shape may be very complex and, e.g., may have a double-pulse structure.

In addition, it may be noted that in contrast to the gas harmonics, in our case the phases of all harmonics are inherently mode locked. The simulations show that for our conditions a train of attosecond pulses is generated (this is similar to mode locking of lasers), with peaks of 160 as width which are separated by one laser period, i.e., 1.3 fs. Such time structures will be the subject of future investigations.

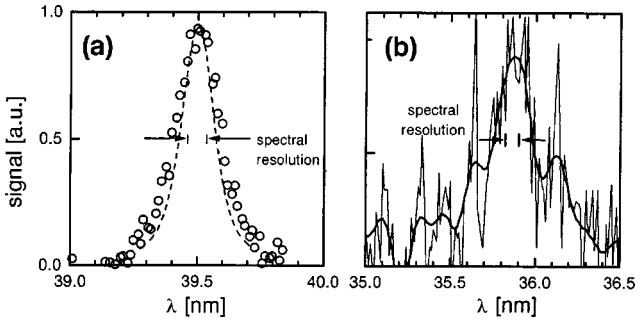

FIG. 13. Measured line profiles from spectrum in Fig. 2(c): (a) 10th harmonic (normal line; circles), (b) 11th harmonic (minimum line). Due to the weak signal the raw data of the 11th harmonic are very noisy (thin line) and thus were smoothed (thick line). The arrows indicate the spectral resolution. For comparison the dashed line in (a) shows the convolution of the simulated line from the oscillating mirror model with a 0.1 nm Lorentzian corresponding to the spectrometer function during the measurement.

VI. CONCLUSIONS

In conclusion, we have reported on measurements of high-order harmonics generated by the interaction of high-intensity high-contrast femtosecond laser pulses with solid targets. Harmonics up to 18th order of the 395 nm fundamental have been observed nonambiguously. Up to date, these are the shortest wavelength FSI harmonics.

Depending on the harmonic order, approximately 10^{-5} to 10^{-4} of the laser energy can be converted to an individual harmonic which is one or two orders of magnitude larger than the previously reported values of FSI harmonics or gas harmonics, respectively. Thus the harmonics are very intense. The measured strong scaling of the harmonic intensity with laser intensity, in particular for the highest orders, in the future may even lead to much stronger radiation and even shorter wavelength harmonics should appear. Thus, in general, due to the ultrashort pulse duration of the individual harmonics estimated from our simulations, HOHG from FSI is very promising for *ultrashort powerful* coherent XUV pulses that may be used for applications. Even shorter pulses, i.e., a train of attosecond pulses, can be expected by collecting several or all of the inherently phase-locked harmonics together.

Moreover, in contrast to the expected well-known continuous roll-off of the high-harmonic orders, the measured spectra show an anomaly. In particular, the harmonic intensity decreases with the increase of harmonic order, but in between shows relative minima which are significantly less intense than the neighboring harmonics. Furthermore, the intensity of the harmonics and the position of the minima depend on the experimental conditions, in particular, on target material. Clear minima with strong emission into high harmonics (up to $N=15$ to 17) above the minimum were observed with carbon and glass targets, but not with the metallic aluminum and copper targets, which show the normal ''roll-off'' behavior.

Additional simulations using a PIC code and the oscillating mirror model show that the physical origin of these modulations is an intricate interplay of resonance absorption and ponderomotive force. It could be shown that this leads to a complicated oscillation of the critical surface. Depending on the actual plasma conditions, the relative contributions of the two dominant oscillation amplitudes X_ω and $X_{2\omega}$ change and hence also the intensity of the harmonics and the positions of the minima as observed in the experiment. In particular, this may also explain the dependence of the minima on the target material.

These explanations are supported by the simulated and observed spectral shapes of the harmonic lines which are in agreement. The shapes of the normal lines correspond to that of the fundamental, with a width that is slightly larger than what is expected from simple nonlinear optics. The minimum lines have a more complicated structure and show wings, which are likely to interference effects originating from the complex motion of the oscillating mirror. Thus, based on our physical picture that points out the complexity of the critical surface oscillation and shows interference effects, it is a challenge to develop a more comprehensive theory, as planned in future.

ACKNOWLEDGMENTS

The authors would like to thank D. Klöpfel for technical support and W. Fölsner for careful target preparation. We gratefully acknowledge G. Tsakiris for discussions. This work was supported by the Deutsche Forschungsgemeinschaft (DFG Grant No. TE 190/2).

[1] V. T. Platenko and V. V. Strelkov, Quantum Electron. **28**, 564 (1998).
[2] M. Gavrila, *Atoms in Intense Laser Fields* (Academic Press, Boston, 1992).
[3] Ch. Spielmann, N. H. Burnett, S. Sartania, R. Koppitsch, M. Schnürer, C. Kan, M. Lenzner, P. Wobrauschek, and F. Krausz, Science **278**, 661 (1997).
[4] Charles G. Durfee III, Andy R. Rundquist, Sterling Backus, Catherine Herne, Margaret M. Murnane, and Henry C. Kapteyn, Phys. Rev. Lett. **83**, 2187 (1999); Ph. Balcou, R. Haroutunian, S. Sebban, G. Grillon, A. Rousse, G. Mullot, J.-P. Chambaret, G. Rey, A. Antonetti, D. Hulin, L. Roos, D. Descamps, M. B. Gaarde, A. L'Huillier, E. Constant, E. Mevel, D. von der Linde, A. Orisch, A. Tarasevitch, U. Teubner, D. Klöpfel, and W. Theobald, Appl. Phys. B: Lasers Opt. **74**, 509 (2002).
[5] R. L. Carman, D. W. Forslund, and J. M. Kindel, Phys. Rev. Lett. **46**, 29 (1981).
[6] M. D. Perry and G. Mourou, Science **264**, 917 (1994).
[7] S. Kohlweyer, G. D. Tsakiris, C.-G. Wahlström, C. Tillman, and I. Mercer, Opt. Commun. **177**, 431 (1995).
[8] D. von der Linde, T. Engers, G. Jenke, P. Agostini, G. Grillon, E. Nibbering, A. Mysyrowicz, and A. Antonetti, Phys. Rev. A **52**, R25 (1995).
[9] R. Lichters, J. Meyer-ter-Vehn, and A. Pukhov, Phys. Plasmas **3**, 3425 (1996); R. Lichters, Ph.D. thesis, Technical University München, 1997.
[10] D. von der Linde and K. Rzàzewski, Appl. Phys. B: Lasers Opt. **63**, 499 (1996).
[11] P. Gibbon, Phys. Rev. Lett. **76**, 50 (1996); IEEE J. Quantum Electron. **33**, 1915 (1997).
[12] P. A. Norreys, M. Zepf, S. Moustaizis, A. P. Fews, J. Zhang, P. Lee, M. Bakarezos, C. N. Danson, A. Dyson, P. Gibbon, P. Loukakos, D. Neely, F. N. Walsh, J. S. Wark, and A. E. Dangor, Phys. Rev. Lett. **76**, 1832 (1996).
[13] J. Zhang, M. Zepf, P. A. Norreys, A. E. Dangor, M. Bakarezos, C. N. Danson, A. Dyson, A. P. Fews, P. Gibbon, M. H. Key, P. Lee, P. Loukakos, S. Moustaizis, D. Neely, F. N. Walsh, and J. S. Wark, Phys. Rev. A **54**, 1597 (1996).
[14] I. Watts, M. Zepf, E. L. Clark, M. Tatarakis, K. Krushelnick, A. E. Dangor, R. M. Allott, R. J. Clarke, D. Neely, and P. A. Norreys, Phys. Rev. Lett. **88**, 155001 (2002).
[15] S. C. Wilks, W. L. Kruer, M. Tabak, and A. B. Langdon, Phys. Rev. Lett. **69**, 1383 (1992).

[16] A. Tarasevitch, A. Orisch, D. von der Linde, Ph. Balcou, G. Rey, J.-P. Chambaret, U. Teubner, D. Klöpfel, and W. Theobald, Phys. Rev. A **62**, 023816 (2000).
[17] M. Zepf, G. D. Tsakiris, G. Pretzler, I. Watts, D. M. Chambers, P. A. Norreys, U. Andiel, A. E. Dangor, K. Eidmann, C. Gahn, A. Machacek, J. S. Wark, and K. Witte, Phys. Rev. E **58**, R5253 (1998).
[18] U. Andiel, K. Eidmann, K. Witte, I. Uschmann, and Förster, Appl. Phys. Lett. **80**, 198 (2002).
[19] U. Andiel, K. Eidmann, and K. Witte, Phys. Rev. E **63**, 026407 (2001).
[20] K. Eidmann, R. Rix, T. Schlegel, and K. Witte, Europhys. Lett. **55**, 334 (2001).
[21] J. Jasny, U. Teubner, W. Theobald, C. Wülker, J. Bergmann, and F. P. Schäfer, Rev. Sci. Instrum. **65**, 1631 (1994).
[22] D. Altenbernd, U. Teubner, P. Gibbon, E. Förster, P. Audebert, J. P. Geindre, J. C. Gauthier, G. Grillon, and A. Antonetti, J. Phys. B **30**, 3969 (1997).
[23] E. L. Benitez, D. E. Husk, S. E. Schnatterly, and C. Tarrio, J. Appl. Phys. **70**, 3256 (1991).
[24] B. L. Henke, P. Lee, T. J. Tanaka, R. L. Shimabukuro, and B. K. Fujikawa, At. Data Nucl. Data Tables **27**, 1 (1982).
[25] In the spectral range shown in Figs. 2 to 5 the reflectivity of the gracing incidence mirror R_m is approximately constant (see, e.g., http://www.cxro.lbl.gov/optical_constants/mirror2.html); the efficiency of TG1 and TG5 is a flat and steady function of wavelength (see, e.g., http://www.cxro.lbl.gov/optical_constants/tgrat2.html).
[26] U. Teubner, C. Wülker, W. Theobald, and E. Förster, Phys. Plasmas **2**, 972 (1995); U. Teubner, W. Theobald, and C. Wülker, J. Phys. B **29**, 4333 (1996).
[27] In Fig. 2(c) weak emission in second diffraction order of TG5 is present: the 11th harmonic (in first order) is sitting on the plasma emission in second order (indicated by "$P2$") which is cutoff at the filter K-edge "$K2$" (second order of "$K1$"). In Figs. 2(a) and 3(c) (TG1) there is no second order background below the minimum.
[28] K. Eidmann, J. Meyer-ter-Vehn, T. Schlegel, and S. Hüller, Phys. Rev. E **62**, 1202 (2000).
[29] U. Teubner, G. Kühnle, and F. P. Schäfer, Appl. Phys. Lett. **59**, 2672 (1991); Appl. Phys. B: Photophys. Laser Chem. **54**, 493 (1992).
[30] T. Wilhein, R. Häßner, D. Altenbernd, U. Teubner, W. Theobald, E. Förster, and R. Sauerbrey, J. Opt. Soc. Am. B **15**, 1235 (1998); A. Saeman and K. Eidmann, Rev. Sci. Instrum. **69**, 1949 (1998).
[31] P. Gibbon, IEEE J. Quantum Electron. **QE-33**, 1915 (1997).
[32] The situation may be different for the interaction of gaseous media with a few cycle laser pulses such as measured by Spielmann *et al.* [3].
[33] A. Bourdier, Phys. Fluids **26**, 1804 (1983).
[34] S. V. Bulanov, N. M. Naumova, and F. Pegoraro, Phys. Plasmas **1**, 745 (1994); S. V. Bulanov *et al.*, Phys. Scr. **T63**, 258 (1996).
[35] C. M. Jost, Dissertation, Ludwig-Maximilians-Universität München, 2001.
[36] This is in contrast to M. Zepf, G. Pretzler, U. Andiel, D. M. Chambers, A. E. Dangor, P. A. Norreys, J. S. Wark, I. Watts, and G. D. Tsakiris, in *Superstrong Fields in Plasma*, *Proceedings of the First International Conference, Varenna, Italy, 1997*, edited by M. Lontano *et al.*, AIP Conf. Proc. No. 426 (AIP, Woodbury, NY, 1998), p. 264; however in that work a significant prepulse was present.